Behavior of self-compact reinforced concrete deep beams with small shear span to depth ratio

Hassan Hassan[1,*], *Mu'taz* Medhlom [1], *Mohammed* Hatem[1]

[1]Faculty of Engineering, Al-Mustansiriyah University, Baghdad, Iraq

Abstract. This research is devoted to investigate the experimental and theoretical behavior of deep beams under monotonic two points loading. An experimental program examining six RC deep beams is carried out. The investigated parameters include shear span to depth ratio varying from 1.0 to 0.276. A comparative study is conducted in this paper by using finite element software ANSYS. The experimental and numerical results show that concrete strength and shear span to depth ratio are the two most important parameters in controlling the behavior of RC deep beams. Comparison of experimental results was made with corresponding predicted values using the Strut and Tie procedure presented ACI 318M-11Code and with other procedures mentioned in the literature. It was found that the Strut and Tie procedure presented in ACI 318M-11Code give conservative results as compared with the experimental tested results. The results showed reliability of analysis in predicting deep beams behavior in terms of failure load, failure mode as well as crack propagation.

1 Introduction

Reinforced concrete (RC) deep beams are structural members for which the load is applied at a distance from the support so that a substantial proportion of the load is transferred directly to the support by arching action. Common structural applications of deep beams include transfer girders in buildings, bridges, and offshore structures. Acording to ACI 318-14 [1]. "Deep beams are members that are loaded on one face and supported on the opposite face such that strut-like compression elements can develop between the loads and supports and that satisfy (a) or (b): (a) Clear span does not exceed four times the overall member depth *h*; (b) Concentrated loads exist within a distance 2*h* from the face of the support." On the other hand, Eurocode 2 (EC2) [2] defines deep beams as all beams with span to depth ratio smaller than three.

The strength of deep beams is usually controlled by shear rather than flexure [3]. As the shear behavior of RC members is still not well understood and is influenced by many parameters, existing design models rely on empirical equations [3, 4]. Even though such approaches are generally extremely conservative, [5-8] they can also lead to unsafe design solutions [8-10]. Therefore, the provisions of current codes of practice need to be reviewed and improved to account for parameters affecting shear behavior and capacity of RC deep beams.

Self-Compacting Concrete (SCC), which flows under its own weight and does not require any external vibration for compaction, has revolutionized concrete placement. SCC first introduced in the late 1980's by Japanese researchers [11], is highly workable concrete that can flow under its own weight through restricted sections without segregation and bleeding. Such concrete should have a relatively low yield value to ensure high flow ability, a moderate viscosity to resist segregation and bleeding, and must maintain its homogeneity during transportation, placing and curing to ensure adequate structural performance and long term durability [12].

2 Research significance

This work aims to provide experimental evidence on the behavior of RC deep beams to enable a better understanding of the effects of shear span-depth ratio, and lead to improved design procedures. The results will also allow an evaluation of the current code provisions and help identify their limitations.

3 Experimental program

The experimental program consists of testing 6 simply supported deep beams under two point loads to investigate the behavior of reinforced concrete deep beams. All beams have the same dimensions and flexural reinforcement. They had an overall length of 1000 mm, a width of 100 mm and a height of 400 mm. The amount of flexural reinforcement for all the tested beams was 3Φ16 mm (ρ=0.0185), as shown in Figure1. Table (1) show details of the six tested reinforced concrete deep beams.

* Corresponding author: hassanfalah@uomustansiryah.edu.iq

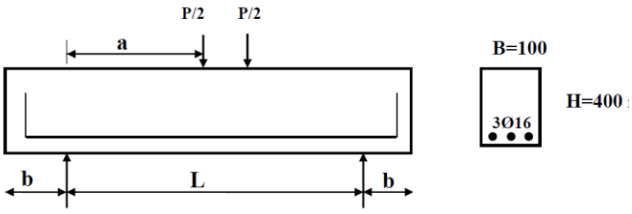

Fig. 1. Details of beam.

Table 1.Specimen details.

Beam No.	L mm	a mm	b mm	d mm	ρ %	a/d
S1	824	362	38	362	1.85	1.0
S2	700	300	100	362	1.85	0.828
S3	580	240	160	362	1.85	0.663
S4	500	200	200	362	1.85	0.552
S5	400	150	250	362	1.85	0.414
S6	300	100	300	362	1.85	0.276

3.1 Materials

Properties and description of used materials are reported and presented in Table (2) and the concrete mix proportions are reported and presented in Table (3).

Table 2. Properties of materials.

Material	Descriptions
Cement	Ordinary Portland Cement (Type I)
Sand	Natural sand from Al-Ukhaider region with maximum size of (4.75mm)
Gravel	Crushed gravel of maximum size (10 mm)
Superplasticizer (S.P.)	Sika Visco Crete PC-20 was used as an admixture to produce SCC in this study
Limestone Powder (L.P.)	Limestone powder from Al-Mousel district is less than 0.125 mm, which satisfies EFNARC 2002[13] recommendations
Reinforcing Bars	(ϕ16mm) deformed steel bar, having (630MPa) yield strength (fy)
Water	Clean tap water

Table 3. Mix prportions

Cement (Kg/m^3)	Sand (Kg/m^3)	Gravel (Kg/m^3)	S.P. (lit/m^3)	L.P. (Kg/m^3)	Water
520	790	750	10	150	0.35

3.2 Fresh SCC properties results

Table (4) illustrates the results of these three tests that carried out on SCC mix and the comparisons with the standard limitations are also presented. From this table, one can notice that the results of all test mixes satisfy the requirements of EFNARC [13] specifications.

3.3 Hardened SCC mechanical properties results

Table (5) shows test results of mechanical properties obtained for SCC mix. These properties are concrete compressive strength (f'c), splitting tensile strength (ft) and modulus of rupture (fr). Each value presented in this table represents the average value of three specimens.

Table 4. Results of fresh SCC

Mix	Slump flow (mm)	T_{50} (sec)	L – box (H_2/H_1)
SCC	700	3	0.85
Limits of EFNARC[13]	650-800	2-5	0.8-1

Table 5. Mechanical properties of hardened SCC

Mix Name	f'_c (MPa)	f_t (MPa)	f_r (MPa)
SCC	50	4.1	5.6

3.4 Test results of deep beams

3.4.1 Ultimate and First Cracking Load

Table (6) summarizes the results of first cracking load (Pcr) and ultimate load (Pu) for all tested beams together with their modes of failure.

Table 6. Results of deep beam

Beam No.	ρ %	a/d	P_{cr} kN	P_u kN	Mode of shear failure
S1	1.85	1.0	25	123	Diagonal tension failure
S2	1.85	0.828	26	152	(Shear +flexural) failure
S3	1.85	0.663	40	190	(Shear +flexural) failure
S4	1.85	0.552	74	245	Diagonal tension failure
S5	1.85	0.414	85	320	Diagonal tension failure
S6	1.85	0.276	90	330	Diagonal tension failure

3.4.2 Load-Mid Deflection Relationships

From the load mid-span deflection relationship shown in Figure 2 for all deep beams, the following three distinct stages are observed:

1. The first stage shows linear behavior with constant slope.
2. In the second stage, vertical flexural cracks were initiated at the tensile face within the maximum bending moment region of the beam, and extend upward, then inclined cracks originated in the shear spans. These cracks developed with increased load, causing a corresponding shift of the neutral axis towards the compression face, and consequently, a continuous reduction in the moment of inertia of the

cracked section. The curve changed from linear to non-linear behavior in this stage.

3. In the third stage, the shape of the load-deflection curve tends to be asymptotic to the horizontal as the beam approached its ultimate load.

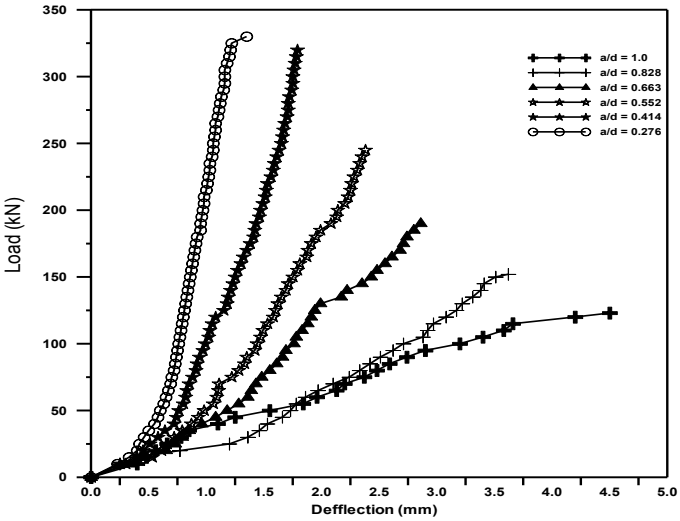

Fig. 2. Load mid-span defelection of beams

3.5 Failure mode

Figure 3 shows the crack patterns after testing all the beams to failure. This plate shows that the failure mode for most of the deep beams tested was through a diagonal shear crack with different widths extending from the bottom of beam near the support to the loading points at the top with different widths. The cracks were accompanied, in some specimens, by the formation of new inclined cracks parallel to the initial cracks in the shear span. However, three specimens failed by flexural vertical cracks extended to the compression zone. The diagonal cracks extended towards the beam's bottom at or near the supports and the loading points at the top but did not reach both.

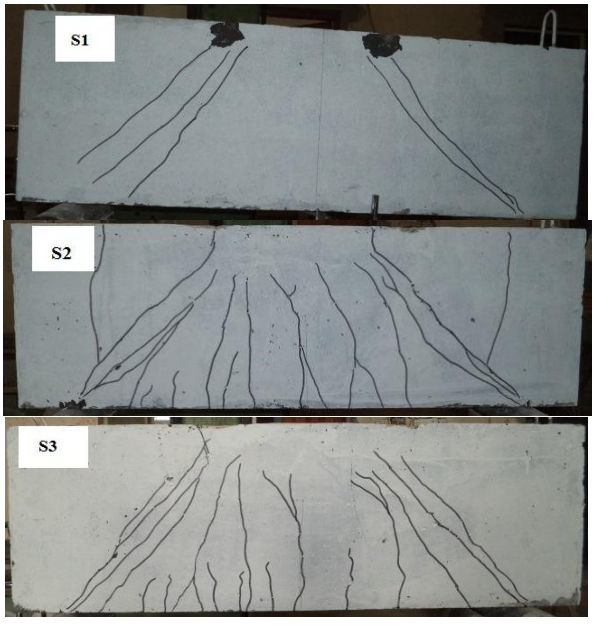

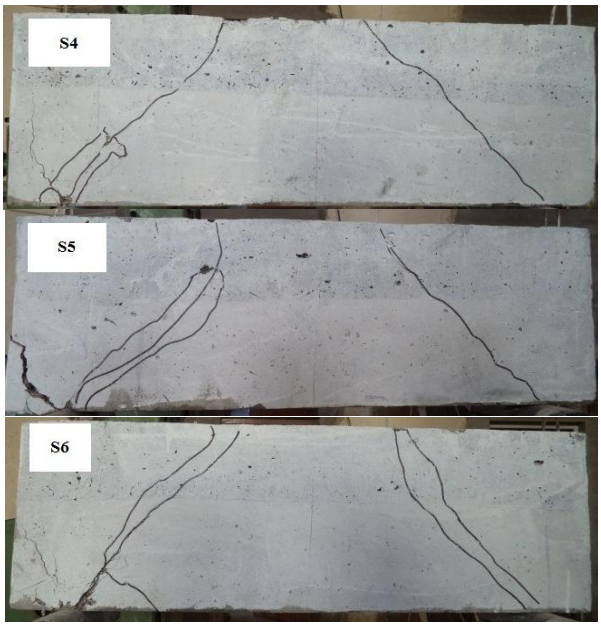

Fig. 3. CRACK PATTERNS AND MODES OF FAILURE

4 Analytical program

4.1 Strut and tie model in design

The strut-and-tie model is a simple equilibrium model based on the lower-bound solution of the plasticity theory and can be used to design D-regions such as deep beams. Design based on the strut-and-tie model (STM) is allowed in all four major international codes: ACI 318-14[1], AASHTO LRFD[14] EC2[2] and Model Code 2010[15] The first step in designing with the STM is to select an appropriate strut-and-tie layout and define the size of each element (Figure 4). Subsequently, the stresses in each element, which should not exceed the maximum allowable stresses, are calculated. Codes of practice give provisions on allowable stresses but do not provide guidance on how to determine the size of the resisting strut and- tie elements, such as struts and nodal regions. As this information is needed to determine the resisting capacity of each element, designers are required to make arbitrary decisions on the size of the elements that transfer the imposed loads to the supports. The STM shown in Fig. 1 can generally be used to analyze all beams with and without shear reinforcement. Sagaseta and Vollum[8] proposed a different STM to account for the effect of shear reinforcement on the strut configuration. This work, however, is not discussed in the current paper, as codes of practice do not suggest the use of different configurations of struts to account for the effect of shear reinforcement. The height of the bottom node (hB) (refer to Figure 4) can be assumed as twice the distance between the center of force of the main longitudinal reinforcement and the tension face. According to Yang and Ashour[16] the height of the top node (hT) can be determined from the equilibrium between the limit of resultant compressive force at the top node (C-C-C), and the limit of resultant tensile force of the bottom node (C-C-T). According to this hypothesis, the height of the top node (hT) is equal to

80%, 88%, 85%, and 75% of the height of the tie according to ACI 318-14[1], AASHTO LRFD[14], EC2[2], and Model Code 2010[15], respectively, while the strut angle (θ) can be calculated from geometry using Eq. (1).

The top and bottom width of the inclined strut (WST and WSB) can be calculated using Eq. (2) and (3)[1] respectively.

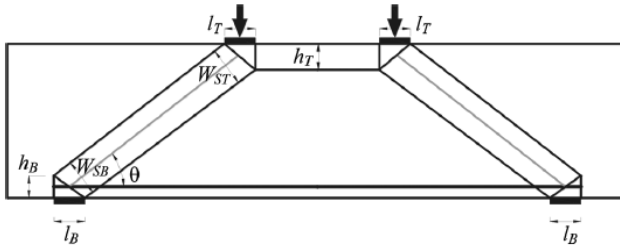

FIG. 4. TYPICAL STRUT-AND-TIE MODEL USED TO PREDICT LOAD CAPACITY OF TESTED BEAMS.

$$\theta = tan^{-1}\left[\frac{d-{}^{h_t}/_2}{a}\right] \quad (1)$$

$$W_{ST} = l_T sin\theta + h_T\, cos\theta \quad (2)$$

$$W_{SB} = l_B sin\theta + h_B cos\theta \quad (3)$$

Cracked RC is an orthotropic material, for which its principal stresses can be assumed to have the same directions of the principal tensile and compressive strains. The presence of lateral tensile strain in the concrete strut, however, can reduce its compressive strength. This is accounted for by using an effectiveness factor to calculate an effective concrete compressive strength. According to ACI 318-14[1], the effective concrete strength (fce) can be calculated using Eq. (4a) while AASHTO LRFD[14], EC2[2], and Model Code 2010[15] use Eq. (5a), Eq. (6a), and Eq. (7a), respectively.

$$f_{ce} = 0.85\beta_s f'_c \quad (4a)$$

Where βs is 0.75 for strut with shear reinforcement satisfying
Eq. (4b); otherwise, βs is taken as 0.6.

$$\sum \frac{A_{si}}{b_s S_i} sin\alpha_i \geq 0.003 \quad (4b)$$

where A_{si} is the area of the reinforcement at spacing si in the
i-th layer of reinforcement crossing a strut at an angle αi to
the axis of the strut.

$$f_{ce} = \frac{f'_c}{0.8+170\varepsilon_i} \leq 0.85 f'_c \quad (5a)$$

Where

$$\varepsilon_i = \varepsilon_s + (\varepsilon_s + 0.002)cot^2\alpha_s \quad (5b)$$

Where αs is the smallest angle between the strut and adjoining
tie; and εs is the tensile strain in the direction of the tie.

$$f_{ce} = 0.6v' f_{cd} \quad (6a)$$

Where v′ can be calculated according to Eq. (6b); and fcd is the design concrete compressive strength.

$$v' = 1 - \frac{f_{ck}}{250} \quad (6b)$$

$$f_{ce} = k_c f_{cd} \quad (7a)$$

$$k_c = 0.55\left(\frac{30}{f_{ck}}\right)^{1/3} \leq 0.55 \quad (7b)$$

The strut-and-tie model shown in Figure 4 with the aforementioned element size definitions will be used for the analysis of the experimental results obtained from the program presented in this paper.

4.2 Modified STM theory

Zhang and Tan [17], suggested a modified STM for calculation of shear strength of reinforced concrete deep beams based on a previous fulfillment reported by Tan and Cheng [18]. For simply supported reinforced concrete beams subjected to symmetric two point loads, from the structural analysis it is well known that the ultimate load (P) is equal to twice the shear force at the support.

$$P = 2V_n \quad (8)$$

The expression for calculated the shear strength Vn according to Zhang and Tan [17], is as follows:

$$V_n = \frac{1}{\frac{4\ \sin\theta_s \cos\theta_s}{A_c f_t} + \frac{\sin\theta_s}{A_{str} f'_c}} \quad (9)$$

where;
Vn: shear strength of deep beams (N).
Ac: is the beam effective cross- sectional area in mm2, equals
to bw dc.
dc: effective beam depth (mm).
Astr: cross-sectional area of the concrete diagonal strut in mm2,
equal to ws bw
ws: effective width of the inclined strut (mm).
bw: width of deep beam (mm).
ft: combined tensile strength of reinforcement and concrete
(MPa).

θ_s: angle between the axis of the strut and the horizontal axis
of the member.

It can be noted that the expression ft is the composite tensile strength including contributions from concrete and reinforcement (web and main bars), where;

$$f_t = f_{ct} + f_{st} \quad (10)$$

f_{ct}: represents the contribution of concrete tensile strength.
f_{st}: represents the contribution of steel reinforcement which
consists of two parts, f_{sw} from the web reinforcement and from the longitudinal reinforcement f_{ss}.

The expression fss refers to the contribution of bottom longitudinal steel, it can be obtained according to the following equation:

$$f_{ss} = \frac{4A_s f_y \sin\theta_s}{A_c/\sin\theta_s} \qquad (11)$$

Where:
A_s: total areas of bottom longitudinal main reinforcement
(mm2).
f_y: tensile yield strength of main reinforcement (MPa).

The performance of the four codes of practice and Zhang in predicting the shear capacity of specimens with a different shear span-depth ratio, and the prediction values are given in Table 7.

5 Theoretical program

To study the structural behavior of the tested beams thoroughly, three dimensional finite element analyses by using ANSYS (version-15) software. The theoretical study includes, in additional to verifications of all experimental beams, modeling and analyzing of twelve additional beam specimens. A nonlinear, eight nodes brick element, (SOLID-65), with three translations DOF at each node is used to model the SCC. For FEM modeling of the steel reinforcement, two nodes, discrete axial element, (LINK-180), with three translations DOF at each node is used. In ANSYS software, the real constants such as cross-sectional area and thickness are needed to represent the geometrical properties of the used elements. While, the material properties are needed to represent behavior and characteristics of the constitutive materials which depends on mechanical properties such as yield stress, modulus of elasticity, Poisson`s ratio and stress-strain relationship. However, each element has a number of fundamental parameters that are identified in the element library of ANSYS. The use of a rectangular mesh is recommended to secure good results from the concrete element (Solid-65), therefore, a rectangular meshing was applied to model all beam specimens. In spite of volumes meshing for concrete and while volumetric and real meshing are used for the concrete media, no meshing was needed for LINK-180 elements because individual elements were introduced in the model through the nodes created by volumetric meshing of the concrete.

The meshing of concrete elements for and alignments of the steel reinforcing bars beams is shown in Figure 5.

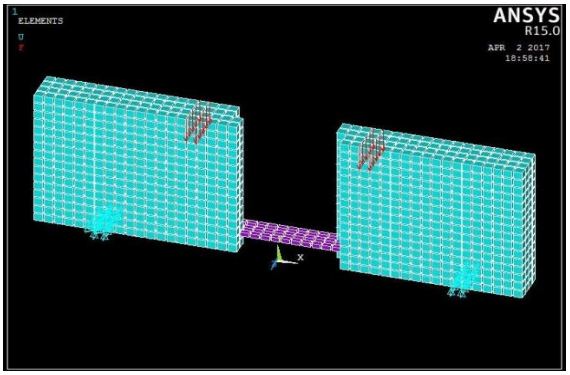

FIG. 5. CONCRETE MESHING AND MODELING OF STEEL BARS

5.1 Ultimate loads

Table 8 shows the comparison between the ultimate loads of the experimental (tested) beams,V_{exp} , and the final loads from the finite element models,V_{num}. The final loads for the finite element models are the last applied load steps before the solution starts to diverge due to numerous cracks and large deflections. It can be observed that there is a simulation between the finite element analysis and the experimental about (93%) for ultimate load capacity, and about (86%) for ultimate deflection and these ratios are considered reasonable and accepted.

5.2 Crack patterns

Crack patterns obtained from the finite element analysis and the failure modes of the experimental beams agree well, as shown in Figure 6. The appearance of the cracks reflects the failure mode for the beams. The finite element model accurately predicts that the beams fail in shear. The cracks were concentrated in the shear span region and vanish diagonally towards the beam supports.

5.3 Parametric study

The parametric study presented here consists of modeling and analyzing of twelve additional beam specimens using ANSYS software. The considered parameters in this study are concrete compressive strength (f'c), the vertical and skin shear reinforcement. The parametric study parameters are reported and presented in Table 9.

5.3.1 Effect of Concrete Compressive Strength

shown in Table 10. It can be noted that the increase in the value of the compressive strength (*fc'*) from (50MPa) to (100MPa) and due to arching action, concrete compressive strength is a dominant parameter influencing the shear capacity of RC deep beams. Figure 7shows the effect of concrete compressive strength on the ultimate capacity of deep beams. The results show that shear capacity of deep beams increases with increasing concrete compressive strength, and this enhancement is more pronounced for beams with smaller shear span-depth ratios.

Table 7: ANALYTICAL SHEAR STRENGTH PREDICTIONS AGAINST EXPERIMENTAL DATA

Beam No.	V_{exp}, kN	ACI 318-14	AASHTO LRFD	EC2	Model Code 2010	Zhang and Tan
		V_{exp}/V_{cal}	V_{exp}/V_{cal}	V_{exp}/V_{cal}	V_{exp}/V_{cal}	V_{exp}/V_{cal}
S1	61.5	0.65	1.31	0. 84	0.87	1.25
S2	76	0.71	1.1	0.89	0.94	1.17
S3	95	0.8	1.06	0.92	0.95	1.09
S4	122.5	0.84	0.84	0.98	1.05	1.00
S5	160	0.87	0.75	0.99	1.08	0.91
S6	165	0.89	0.73	1.03	1.13	0.85
Average		0.793	0.965	0.941	1.003	1.045
Standard deviation		0.08	0.2	0.06	0.09	0.14
C.O.V		0.12	0.24	0.075	0.098	0.15

Table 8: NUMERICAL AND EXPERIMENTAL RESULTS

Beam No.	ρ %	a/d	P_{exp} kN	Δ_{exp} mm	ANSYS	
					P_{exp}/P_{num}	$\Delta_{exp}/\Delta_{num}$
S1	1.85	1.0	123	4.5	0.93	0.8
S2	1.85	0.828	152	3.62	0.92	0.87
S3	1.85	0.663	190	2.86	0.91	0.84
S4	1.85	0.552	245	2.38	0.95	0.9
S5	1.85	0.414	320	1.79	0.95	0.88
S6	1.85	0.276	330	1.4	0.93	0.87
Average					0.93	0.86
Standard deviation					0.016	0.032
C.O.V					1.09	2.17

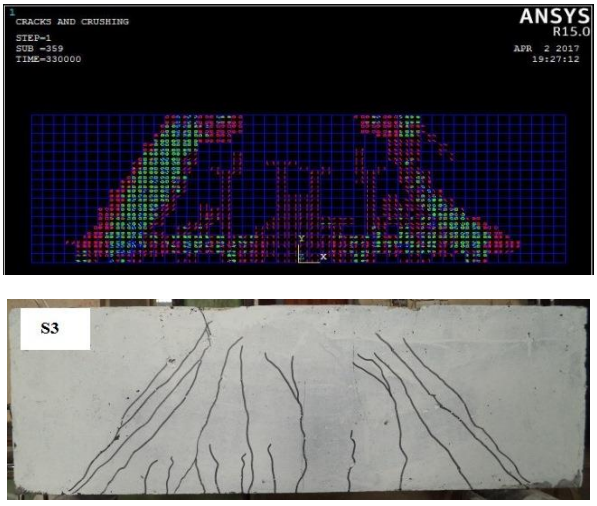

FIG. 6. CRACK PATTERNS COMPRESSION

Three grades of concrete compressive strength have been used. The numerical results of ultimate load capacity (P_{num}) and the corresponding deflection (Δ_{num}), are

5.3.2 Effect of Vertical and Skin Shear Reinforcement

Two ratios of shear reinforcement have been used. The numerical results of ultimate load capacity (P_{num}) and the corresponding deflection (Δ_{num}), are shown in Table 11. The increase in shear reinforcement ratio from 0 to 0.4% led to an increase in load capacity. This can be attributed to the fact that the vertical shear reinforcement can carry directly a portion of the applied shear force and provide confinement to the concrete, thus allowing the development of higher compressive stresses. In addition, both vertical and skin reinforcements can reduce crack opening, thus increasing the contribution to shear resistance offered by the concrete through aggregate interlock. Figure 8 shows the effect of shear reinforcement on the ultimate capacity of deep beams.

Table 9: EFFECT OF SHEAR REINFORCEMENT ON ULTIMATE LOAD AND DEFLETION

Beam Designation	a/d	Vertical & Horizontal shear reinforcement %	p_{num} kN	Δ_{num} mm
S1	1	0	114	3.6
S1-0.2	1	0.2	155	3.5
S1-0.4	1	0.4	190	3.46
S2	0.828	0	140	3.1
S2-0.2	0.828	0.2	188	3.07
S2-0.4	0.828	0.4	245	2.99
S3	0.663	0	173	2.4
S3-0.2	0.663	0.2	209	2.31
S3-0.4	0.663	0.4	289	2.26
S4	0.552	0	233	2.14
S4-0.2	0.552	0.2	267	2.08
S4-0.4	0.552	0.4	310	2.02
S5	0.414	0	304	1.57
S5-0.2	0.414	0.2	348	1.5
S5-0.4	0.414	0.4	399	1.42
S6	0.276	0	307	1.2
S6-0.2	0.276	0.2	345	1.11
S6-0.4	0.276	0.4	410	1.03

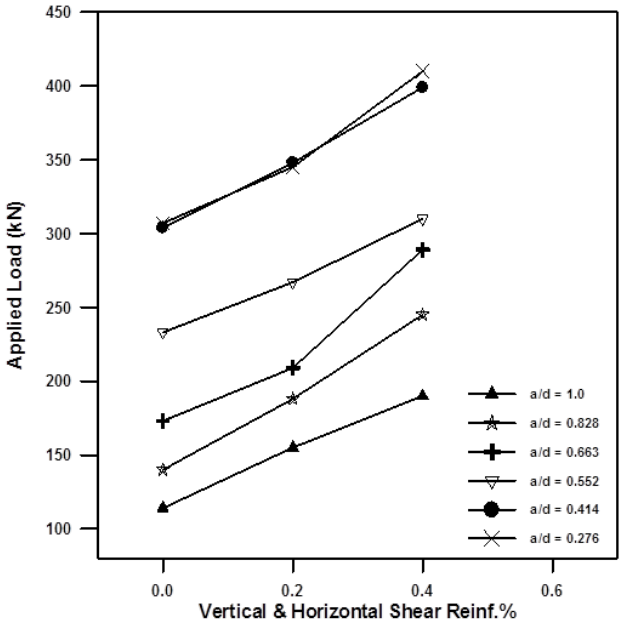

FIG. 7 EFFECT OF SHEAR REINFORCEMENT ON ULTIMATE FAILURE LOAD.

6 Conclusions

On the basis of the experimental and theoretical results presented in this study and the assessment of different design approaches, the following conclusions can be drawn:

1. As a/d ratio, reduces the arch action becomes more dominant whereby loads are transferred directly by arch in compression. Thus the conventional plane-sectional shear approach is inappropriate for deep beams.
2. Concrete compressive strength has more influence on the shear strength of deep beams than shear reinforcement. However, the presence of shear reinforcement is crucial in controlling crack propagation and providing ductility to deep beams.
3. The effectiveness factor is dominated by concrete compressive strength but it is also influenced by the shear span-depth ratio. ACI 318-14 provisions neglect the effect of these two parameters in estimating the effective concrete strength of the inclined strut and, as a result, lead to unconservative predictions.
4. Shear strength predictions by the STM with the provision of AASHTO LRFD generally yield more conservative results among the examined codes.
5. Shear strength predictions by the STM with the provisions of both EC2 and Model Code 2010 are generally conservative; however, their conservatism reduces with increasing shear span-depth ratio because these two codes neglect the effect of shear span-depth ratio on the concrete effectiveness factor.
6. The predicted load by ANSYS in deep beams at various stages was found to be in good agreement with the test data. Where the estimated deflection of beam at ultimate load was much closer to the experimental data.

References

1. ACI Committee 318, “Building Code Requirements for Structural Concrete (ACI 318M-14) and Commentary (ACI 318RM-14),” American Concrete Institute, Farmington Hills, MI, 520 pp (2014)

2. British Standards Institution, “Eurocode 2: Design of Concrete Structures: Part 1-1: General Rules and Rules for Buildings,” British StandardsInstitution, London, UK, 97 pp (2004)

3. K. Smith, A. Vantsiotis, “Shear Strength of Deep Beams,” ACI J. Proceedings, **79**, 3, Mar., pp. 201-213 (1982)

4. M. P. Collins, D. Mitchell, E. C. Bentz, The Struc. Eng., **86**, 10, pp. 32-39 (2008)

5. R. Tuchscherer, D. Birrcher, C. Williams, D. Deschenes, O. Bayrak, ACI Struc. J., **111**, 6, Nov.-Dec. (2014), pp. 1451-1460. doi: 10.14359/516869926

6. A. Arabzadeh, A. Rahaie, R. Aghayari, Inter. J. of Civil Eng., pp. 141-153, **7**, 3 (2009)

7. D. Kuchma, S. Yindeesuk, T. Nagle, J. Hart, H. Lee, ACI Struc. J., **105**, 5, pp. 578-589, Sept.-Oct. (2008)

8. J. Sagaseta, R. Vollum, Magazine of Conc. Research, **62**, 4, (2010), pp. 267-282. doi: 10.1680/macr.2010.62.4.267

9. M. P. Collins, E. C. Bentz, E. G. Sherwood, ACI Struc. J., **105**, 5, pp. 590-600, Sept.-Oct. (2008)

10. M. D. Brown, O. Bayrak, ACI Struc. J., **105**, 4, pp. 395-404, July-Aug. (2008)

11. N. Nagamoto, K. Ozawa, “Mixture properties of Self-Compacting, High-Performance Concrete”, Proceedings, Third CANMET/ACI Inter. Conf. on Design and Materials and Recent Advances in Concrete Technology, SP-172, V. Malhotra, American Concrete Institute, Farmington Hills, p. 623-637, Mich. (1997)

12. K. H. Khayat, A. Ghezal, “Utility of Statistical models in Proportioning Self-Compacting Concrete”, Proceedings, RILEM Inter. Symp. on Self-Compacting Concrete, Stockholm, p. 345-359, (1999)

13. EFNARC: European Federation Dedicated to Specialist Construction Chemicals and Concrete Systems, “Specifications and Guidelines for Self-Compacting Concrete” Association House, 99 West Street, Farnham, Surrey, U.K., 32 pp., Feb. (2002)

14. AASHTO, "AASHTO LRFD Bridge Design Specifications," American Association of State Highway and Transportation Officials, Washington, DC, (2012)

15. International Federation for Structural Concrete, "Model Code 2010 – first complete draft," fib Bulletin No. 55, 288 pp., (2010)

16. K. H. Yang, A. F. Ashour, J. of Struc. Eng., **137**, 10, (2011), pp. 1030-1038. doi: 10.1061/(ASCE)ST.1943-541X.0000351.

17. N. Zhang, K.H. Tan, Science Direct, Engineering Structures J., **29**, pp. 2987-3001, March, (2007)